Applied Clay Science 150 (2017) 309–322

Contents lists available at ScienceDirect

Applied Clay Science

journal homepage: www.elsevier.com/locate/clay

Research Paper

Zn-clay minerals in the Skorpion Zn nonsulfide deposit (Namibia): Identification and genetic clues revealed by HRTEM and AEM study

Giuseppina Balassone[a,*], Fernando Nieto[b], Giuseppe Arfè[a], Maria Boni[a], Nicola Mondillo[a]

[a] Dipartimento di Scienze della Terra, dell'Ambiente e delle Risorse, Università degli Studi di Napoli Federico II, Napoli, Italy
[b] Departamento de Mineralogía y Petrología and IACT, Universidad de Granada, CSIC, Granada, Spain

ARTICLE INFO

Keywords:
Zn-smectite
Sauconite
Skorpion
Namibia
HRTEM
AEM

ABSTRACT

Zn-clays worldwide occur in various supergene nonsulfide (Zn-Pb) ores, where they can be the prevailing economic minerals or represent minor concentrations in the mineral assemblage. The world-class Zn smectite-rich Skorpion mine (Namibia) is considered one of the most important supergene nonsulfide zinc deposits in the world. At Skorpion, the trioctahedral Zn-bearing smectite predominates over the other Zn-oxidized minerals. This work is focused on microtextural observation and chemical analyses on the clay nano-particles of the supergene nonsulfide ores from Skorpion, carried out for the first time using TEM/HRTEM and AEM investigations. This approach helped to better understand the formation mechanism of the Skorpion Zn-clays and related phases down to the nanoscale. The microtextures of the Skorpion Zn-clays suggest they formed from fluids, meteoric and/or hydrothermal in nature, in two textural contexts: smectites can grow on previously deposited phyllosilicates (mica) (CCP texture), and/or directly nucleate from Zn-rich solutions (PCA texture). The Skorpion sauconite is chemically characterized by a greater homogeneity if compared with natural sauconites from other occurrences; it is quite stoichiometric, with Ca as interlayer cation and limited quantities of Mg and Fe, with an average composition of $Ca_{0.14}K_{0.02}(Zn_{2.7}Mg_{0.09}Al_{0.14}Fe_{0.10})(Si_{3.4}Al_{0.6})O_{10}(OH)_2{\cdot}nH_2O$. Contrary to Peru nonsulfide ores (Accha and Yanque), at the micro- and nanoscale the occurrence of Zn-beidellite at Skorpion is very subordinated. Chlorite and baileychlore have been also detected. Detrital micas are commonly the template for epitaxial sauconite growth. Typical supergene processes at ambient temperatures should be considered for the genesis of the Skorpion sauconite-bearing deposit, with some local contribution of low-T hydrothermal fluids. The micro- and nano-features of the Skorpion mineral assemblage confirm the complex mineralogical nature of the smectite-rich nonsulfide (micro)systems, with remarkable implications for mineralogical evaluation and processing.

1. Introduction

Zn-clays occur in various supergene nonsulfide ores worldwide. In these ores, mainly deriving from the weathering of primary sulfide concentrations, the Zn-clays can be the prevailing economic minerals, or represent minor concentrations in the mineral assemblage (Arfè et al. 2017; Boland et al., 1992; Balassone et al. 2008; Boni et al., 2009a, b; Boni and Mondillo 2015; Borg et al. 2003; Buatier et al. 2016; Choulet et al. 2016; Coppola et al. 2008; Emselle et al. 2005; Frondel 1972; Hye In Ahn 2010; Kärner 2006; Mondillo et al. 2014, 2015). Zn-clay minerals, formed in slightly acidic to neutral conditions, are also commonly found in contaminated soils at mining and smelting sites (i.e. Manceau et al. 2000; Juillot et al. 2003).

Sauconite (Ross 1946; Newman and Brown 1987), which is one of the most common clay minerals in nonsulfide deposits, is a trioctahedral saponite-like smectite with Zn in octahedral coordination. Experimental studies on its synthesis and stability (i.e. Higashi et al. 2002; Kloprogge et al. 1999; Pascua et al. 2010; Petit et al. 2008) demonstrated that this Zn-smectite can precipitate from solutions of silicic acid, variously mixed with Zn-compounds (Zn-chloride, Zn-oxide, or Zn-hydroxide) and Na- and Al-compounds, at a pH interval of 6–12 and temperatures ranging between 20 and 200 °C.

Among the other Zn-"clay" phases found in nonsulfide ore deposits, we should mention fraipontite (a serpentine-like Zn-clay mineral, Fransolet and Bourguignon 1975) and baileychlore (a Zn-chlorite, Rule and Radke 1988). Recently Kaufhold et al. (2015) characterized Zn-smectites from the Silver Coin Mine (USA), while Choulet et al. (2016) and Buatier et al. (2016) have described Zn-clays consisting of interstratified fraipontite/smectite (fraipontite-prevailing), closely associated to willemite in several nonsulfide Zn deposits in the Moroccan

* Corresponding author.
E-mail address: balasson@unina.it (G. Balassone).

http://dx.doi.org/10.1016/j.clay.2017.09.034
Received 7 April 2017; Received in revised form 18 September 2017; Accepted 26 September 2017
0169-1317/ © 2017 Published by Elsevier B.V.

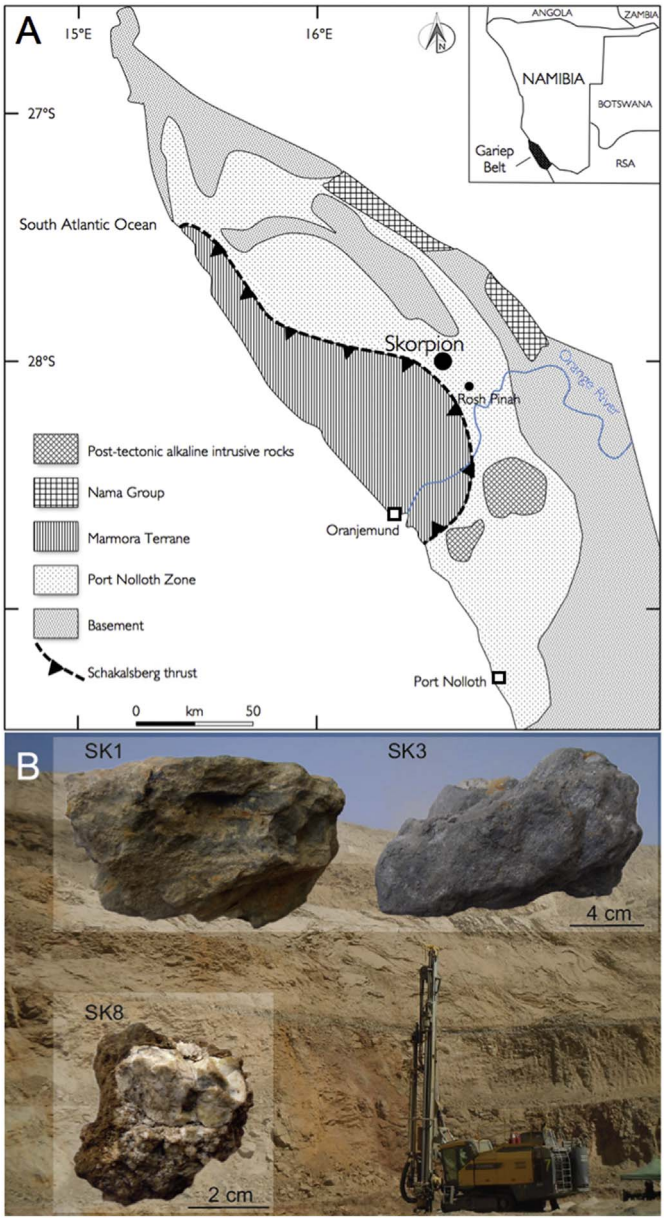

Fig. 1. (A) Schematic geological map of southern Namibia (modified after Borg et al. 2003 and references therein), with location of the Skorpion deposit in the Gariep belt area. (B) The Skorpion open pit at the date of the sampling (2014), with the samples investigated in this study (see text).

High Atlas, which formed by direct precipitation of meteoric and/or hydrothermal fluids. With the increasing quest of mineral resources (and the rising Zn price), mining industries must afford the complex issues related to the extraction and processing of low grade and/or finely disseminated ores. Clay minerals, including Zn-clays that have been detected in several deposits, are not only a resource (the Skorpion case) but can affect the industrial treatment to a various extent (Choulet et al. 2016 and references therein). Hence, their detailed mineralogical study, as well as the investigation of their crystallization and post-crystallization processes can provide crucial geological information, particularly useful from the perspective of industrial and economic evaluations.

One of the best examples of a Zn smectite-rich supergene orebody is the world-class Skorpion mine (Namibia, Vedanta Ltd.) (consisting of 21.4 Mt. of ore reserves, grading 10.6% Zn at the beginning of the exploitation). The Skorpion base metals deposit is considered to have been an equivalent of the Rosh Pinah massive sulfides concentration that was subjected to weathering processes, started after the end of the pan-African tectonic phase (Kärner 2006). The pan-African phase was followed by uplift and denudation, and concluded with the onset of a strong arid period that had its first maximum in Oligocene (Borg et al. 2003; Kärner 2006; Arfè et al. 2017). At Skorpion, the trioctahedral Zn-bearing smectite (sauconite) predominates over the other Zn-oxidized minerals (Borg et al. 2003; Kärner 2006).

The chemical and structural features of sauconite from Skorpion have never been examined in detail before; hence, the present research is focused on microtextural observation and chemical analyses on the clay fraction of the supergene nonsulfide ores, carried out for the first time using TEM-STEM and HRTEM investigations. This approach by means of transmission electron microscopy, coupled with high-resolution observations, integrated with other mineralogical and geochemical analyses, allows the investigation of clay textures down to the nanoscale, and consequently a better understanding of their genesis.

2. Geology of the Skorpion zinc deposit area

The Skorpion zinc deposit (Fig. 1A) is hosted by metamorphosed volcano-sedimentary rocks of the Port Nolloth Zone (PNZ), within the late Proterozoic Gariep Belt (Borg et al. 2003). This belt is subdivided into an eastern para-autochthonous zone, the PNZ, and a western allochthonous zone, the Marmora Terrane. The Gariep Belt is regarded as the southern extension of the Damara orogenic front of central and northern Namibia (Davies and Coward 1982; Reid et al. 1991; Stanistreet et al. 1991; Gresse 1994; Frimmel 2000; Jasper et al. 2000; Frimmel et al. 2002). The rocks of the PNZ contain stratiform Zn-Pb-Cu-Ag-(± Ba)-sulfide mineralization in sedimentary and felsic metavolcanic rocks. The best examples are the Rosh Pinah Pb-Zn (Page and Watson 1976; van Vuuren, 1986; Alchin and Moore 2005) and the Skorpion Zn-(Cu) deposits (Borg et al. 2003; Kärner 2006), which were attributed to either the Volcanic-hosted Massive Sulfides (VHMS) or Sedimentary-hosted Massive Sulfides (SHMS) types. The mineral concentrations were formed in an extensional environment during a phase of increased volcanogenic-hydrothermal activity between 740 and 754 Ma (Borg and Armstrong 2002). The deformation of the ore-bearing units (due to the pan-African tectonic phase) took place during continental collision that produced the closure of the Adamastor oceanic basin 545 million years ago (Alchin and Moore 2005). The sedimentary and bimodal volcanic rocks hosting the mineralization have been strongly folded, faulted and overprinted by a lower amphibolite facies metamorphism (Frimmel et al. 1995). Exhaustive summaries about the geomorphological evolution of southern Africa and Namibia, including the Gariep Belt, which took place after the pan-African tectonic phase (King 1951), have been presented by Partridge and Maud (1987) and Partridge (1998). The maximum peneplanation, coupled with intense lateritic weathering, causing also part of the Skorpion supergene mineralization, was reached between Late Cretaceous and Oligocene. During Late Cretaceous-Eocene, a denudation event eroded a 3 km-thick section of southern Africa and Namibia, reaching several hundred km inland and producing the so-called “African Erosion Surface” (Gallagher and Brown 1999). This surface was then rejuvenated and intersected by younger erosion planes, related to discrete uplifts that took place in early Miocene and Pliocene (Partridge and Maud 1987).

The Skorpion deposit cuts across the deeply weathered Rosh Pinah Formation metavolcanics and the Hilda Subgroup carbonate rocks. The Zn-oxidized minerals are mainly hosted by arkoses and subordinately by quartz-sericite schists of volcanic origin. Other rock types associated with the orebody include limestones and mafic volcanics (Borg et al. 2003; Kärner 2006). The Skorpion nonsulfide orebody is covered by a transported barren regolith, consisting of a surficial layer of wind-blown sand above a massive calcrete layer, covering a sequence of alluvial interlayered gravels and conglomerates. Great part of the oxidized orebody is considered to have been formed in a paleo-channel,

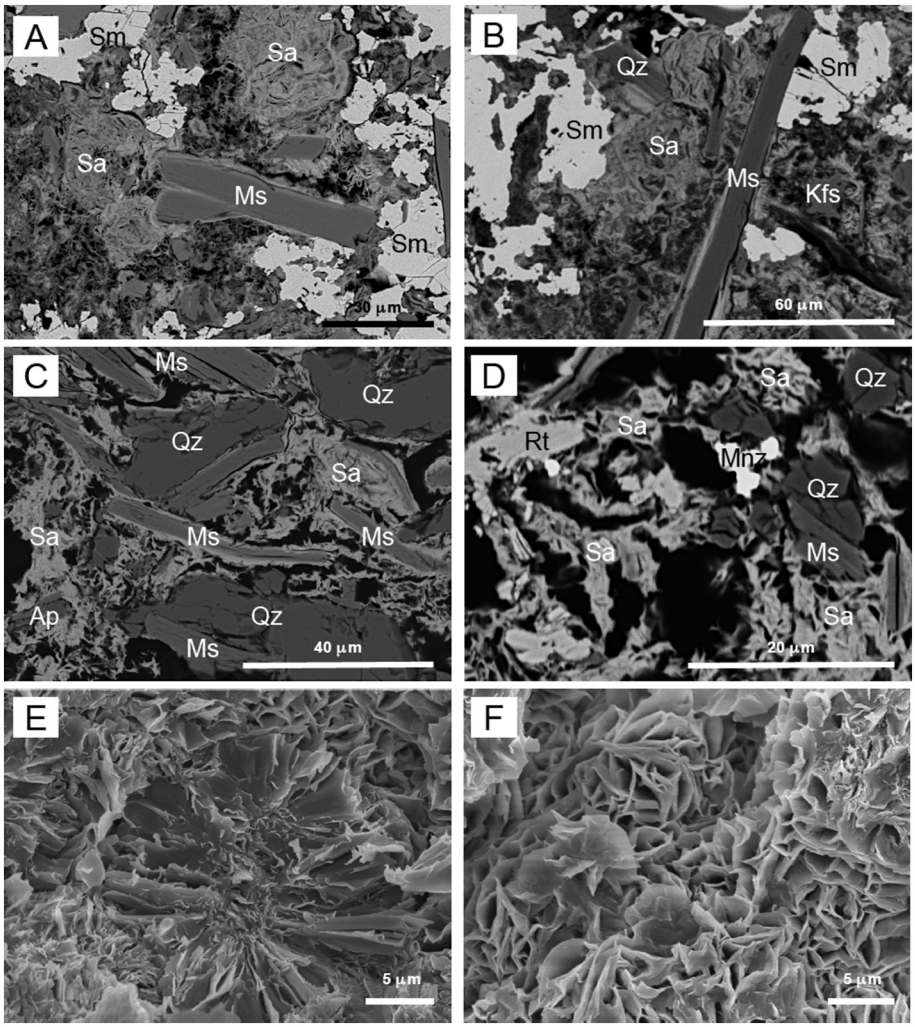

Fig. 2. (A), (B) BSE micrographs of sauconite-bearing sample SK1, and (C), (D) sample SK3; mineral abbreviations (Whitney and Evans 2010): Ap, apatite; Kfs, K-feldspar; Mnz, monazite; Ms., muscovite; Qz, quartz; Rt, rutile; Sa, sauconite; Sm, smithsonite. (E), (F) SE micrographs of smectite in sample SK8, respectively from brownish and white (clay-rich) areas (see Fig. 1B).

after the supergene alteration of the primary orebody associated to an erosional surface (Borg et al. 2003). This surface is most likely an equivalent of the "African Erosion Surface" dated as Cretaceous-Early Tertiary (Partridge and Maud 1987). Major ore minerals at Skorpion include not only smithsonite, sauconite and hemimorphite (Borg et al. 2003), but also other Zn minerals like tarbuttite, scholzite, chalcophanite, hydrozincite, skorpionite, and hydrohetaerolite (Kärner 2006; Arfè et al. 2017; Balassone et al. 2016; this study). A new hydrated yttrium-erbium phosphate has been recently discovered and determined as churchite-Y, i.e. $(Y,Er)PO_4{\cdot}2H_2O$ (Hinder 2015). Based on the stable isotope data of supergene carbonates, Arfè et al. (2017) suggested that the nonsulfide mineral assemblage precipitated at an average temperature of 17 °C, either during the first (Late Cretaceous-Paleocene), or the last humid climatic stage (early-middle Miocene).

The formation process of the Skorpion Zn-bearing supergene minerals, among which sauconite, started from the oxidation of primary (hypogene) sulfides (sphalerite, pyrite, minor chalcopyrite and galena), hosted in late Proterozoic felsic metavolcanic and metasiliciclastic rocks (Borg et al. 2003; Kärner 2006). The oxidation of primary sulfides (mainly pyrite) within these host rocks produced (i) sulfuric acid, (ii) the release of base metals (Zn^{2+}, Pb^{2+} and Cu^{2+}) transported in initially acidic solutions, and (iii) insoluble iron hydroxides, which testify high Eh/low pH conditions (Scott 1986; Garrels and Christ 1990). The metal-bearing (Zn-dominated) fluids percolated through the rocks were able to dissolve some of their detrital siliciclastic components. i.e. mainly detrital feldspars and micas (as well as the calcite cements), which provided Si and Al, together with alkaline ions, for sauconite formation. The mineral-water reactions of the hydrolysis processes must have buffered the pH of the supergene fluids, since they produced two strong bases, namely NaOH and KOH (Sherman 2001). These bases contributed to the buffering/neutralisation of the acid meteoric fluids, which migrated through the Skorpion metaarkoses. Thus, the supergene fluids became less acidic during the progressive leaching of feldspars from the Late Proterozoic rocks. This neutralisation process played a significant role in the formation of the supergene non-sulfide zinc ore body, giving rise to moderate Eh and pH conditions, favorable for the precipitation of the supergene zinc-bearing minerals, among which sauconite. Its formation requires Eh-pH conditions similar to hemimorphite and smithsonite (i.e. neutral to weak alkaline oxidising), although it can be also stable under weak acid conditions (Kärner 2006, and references therein).

3. Materials and methods

The TEM-AEM study was conducted on three samples (SK1, SK3 and SK8), collected from the Skorpion open pit (Fig. 1B). Preliminary petrographic and mineralogical analysis was carried out in order to identify the main mineral textures and paragenesis. The samples were characterized by X-ray powder diffraction (XRPD), using a Seifert–GE ID3003 diffractometer, with CuKα radiation, Ni-filtered at 40 kV and 30 mA, 3–80°2 range, step scan 0.02°, time 10 s/step, and the RayfleX (GE) software package (Dipartimento di Scienze della Terra, dell'Ambiente e delle Risorse, DiSTAR, University of Naples Federico II). The mineral assemblages were also investigated by polished-thin sections

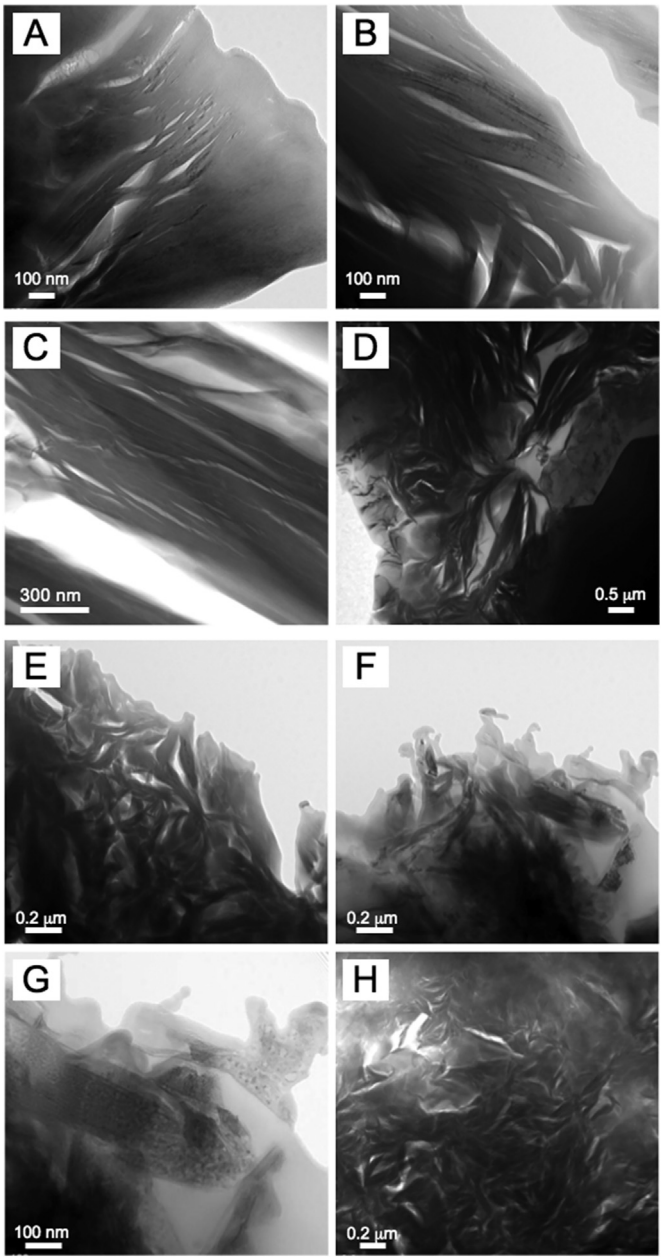

Fig. 3. Textural images of compact clay packages (CCP): (A), (B), (D) sample SK1; (C) sample SK8. Textural images of porous clay packages (PCP): (E), (F) sample SK1, with (G) enlargement of (F); (H) sample SK8.

used for optical microscopy (OM) and scanning electron microscopy with energy dispersive X-ray spectroscopy (SEM-EDS) (DiSTAR, Naples). A JEOL JSM5310 equipped with an Oxford energy dispersive spectrometry (EDS) INCA X-stream pulse processor interfaced with the 4.08 version Inca software has been used. The HRTEM study on thin sections, aimed to investigate the texture of clays at micro- and nanoscale, was performed at the Centro de Instrumentación Cientifica (CIC) of the University of Granada (Spain). Copper rings were attached to representative selected areas of the matrix of thin sections prepared with Canada balsam and after ion-thinned, using a Fischione Model 1050 ion mill, and carbon coated. Ion milling was performed at 4 kV and ± 10°, until the first hole and ± 7° during 20 min for final cleaning. We used a Titan TEM with XFEG emission gun, spherical aberration corrector and HAADF detector, working at 300 kV, with a resolution of 0.8 Å in the TEM mode and 2 Å in the STEM mode. EDX spectra for qualitative identification of minerals and chemical maps were obtained using the Super-X system. Quantitative analyses were obtained using albite, biotite, muscovite, spessartine, olivine, titanite, and hemimorphite as standards, measured using the same protocol as samples, to obtain K-factors for the transformation of intensity ratios to concentration ratios according to Cliff and Lorimer (1975).

Taking into account the analytical difficulties in detecting the Na^+ peak, because of the Na−Zn peaks overlap in the energy-dispersion spectrum, for one sample (SK8) a chemical analysis of the clay fraction (carefully separated and checked for purity by XRD) was carried out by inductively coupled plasma - optical emission (ICP-OES), after a eight-peroxide assay, using a Thermo Jarrell-Ash ENVIRO II ICP (Actlabs, Ancaster). The uncertainty is < 3% for the major oxides and < 5% for all other trace elements (for the precision of the method, see actlabs.com).

4. Results

The mineralogical assemblages of the investigated Skorpion samples, inferred by combined XRPD and SEM-EDS analyses, are always represented by sauconite as main phase. All the X-ray diffraction patterns exhibit the typical reflections of the Zn-smectite, with broad diffraction maxima, indicative of the lack of perfect long-range order due to stacking faults and/or fine grained crystallite dimension, corresponding to the 001 reflections positioned at about 14.72 Å, and the diagnostic 060 reflections centred at ~1.54 Å. Samples SK1 (Fig. 2A, B) and SK3 (Fig. 2C, D) also contain minor amounts of smithsonite, quartz, muscovite, K-feldspar and very rare apatite. Sporadic rutile and monazite were detected only in sample SK3 REE (+ Y) phosphates were also found as secondary REE minerals at Skorpion by Kärner (2006), in highly altered gossaneous metasediments at Skorpion as secondary REE minerals. If compared with the other samples, sample SK8 is particularly rich in sauconite; it is composed of dark-brown parts with sauconite and lesser Fe-oxy-hydroxides (Fig. 1B and 2E), and white parts with prevailing Zn-clay (Fig. 1B and 2F). Minor amounts of quartz and muscovite have been also detected.

4.1. Microtextures of clays and related minerals

Using the ion-milling technique preparation, we were able to observe the mineral fabric of the Zn-clays in the three Skorpion samples which, at low magnification, present similar characteristics and comparable electron diffraction patterns (SAED). The microtextures of the Zn-clays observed in the Skorpion samples at size below 10 μm are very similar to those described by Mondillo et al. (2015) in the Yanque mine (Peru); as a matter of fact, also at Skorpion it was possible to identify the compact clay packages (CCP), as well as the porous clay aggregates (PCA). The CCP type is represented by straight and almost isoriented packets (Fig. 3A-D), with a length up to several micrometres and a thickness below ~1 μm. The packets can locally pass to slightly curved fibres coexisting with the straight packets, as an epitaxial growth onto mica crystals (Fig. 4) or rarely as void fillings. The PCA type consists of very fine-grained packets, with sizes lower than the CCP types, below ~ 400 nm (Fig. 3E-H). This microtexture seems to be less frequent in the studied samples than in CCP, and it is occasionally closely related to Fe-hydroxides (Fig. 3G).

The electron diffraction patterns of the CCP type are shown in Fig. 5A and B; they correspond to a partially collapsed smectite with spacings of ~12 Å between layers, which typically occur as a consequence of TEM vacuum and/or electron irradiation and 5.1 Å in the a* direction. In Fig. 5C the electron diffraction pattern of mica is shown, which represents the substrate on which CCP smectite grew with an epitaxial mechanism, as discussed afterwards. In this sample (i.e. SK3), the rows have a spacing of 20 Å; lattice fringes with spacings of 20 Å are measured for the same area, which identifies the 2 *M* polytype (Fig. 5D). Fig. 5E and F show the high-resolution images of CCP smectite, with lattice fringes ranging between ~12 and 13 Å. In

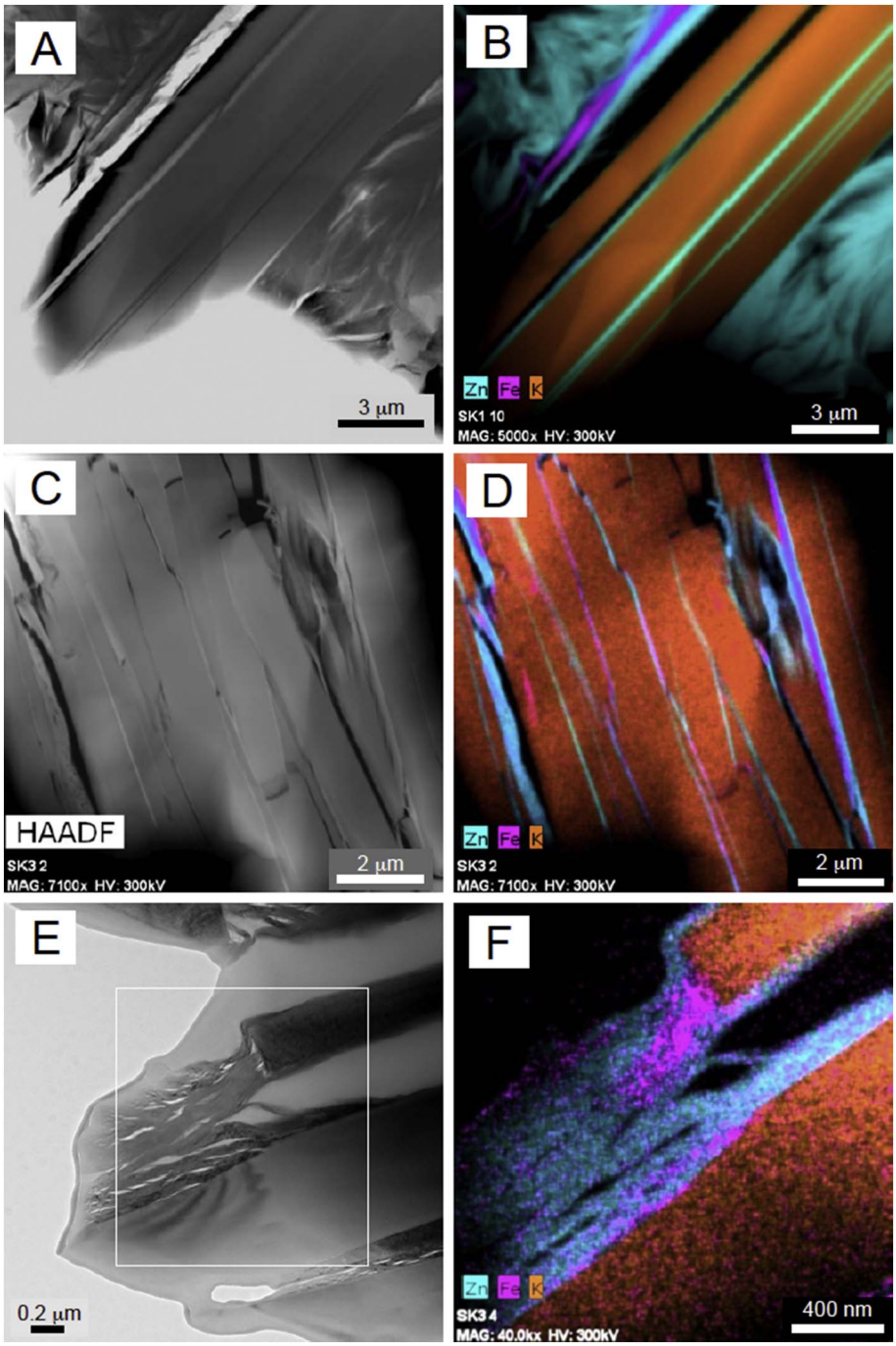

Fig. 4. Epitaxial growth of smectite onto mica: (A), (B) sample SK1; (C), (D), (E), (F) sample SK3. In (B), (D), (F) STEM-EDX spectra of the investigated areas (on the left) are reported, clearly showing the K-rich mica areas and the Zn-rich sauconite ones. (F) Enlargement corresponding to the white frame in (E), where small areas richer in Fe can be also observed (see text).

general, the measured d_{001} values of sauconite vary in a interval of 10.5–13 Å, due to different degrees of collapsing.

As reported in Mondillo et al. (2015), the PCA smectite can be also associated with Fe-oxy-hydroxides. Fig. 6A and B show a HRTEM image with the typical d_{khl} of hematite; the crystalline domains size is very small and disoriented each other, but it is not really defective. In Fig. 6C a small amount of native silver retained in the smectite flakes has been also detected in an area where Fe-oxy-hydroxides and sauconite seem to be finely intergrown; Ag is likely attributable to a pure metal instead to a compound, which is simply retained in the smectite flakes.

In Fig. 7 it is shown how iron minerals are disseminated in the smectite interstices. In the same figure, it is worth noting the occurrence of another phase likely interpreted as a Zn-oxide, due to the small C peak, that would allow excluding a Zn-carbonate. The qualitative EDX spectra show that this mineral also contains a series of metals like Fe, Mn, Co, Ni, Zr, Cd and Pb, not detected elsewhere.

Unlike the Peruvian smectite-rich samples (Mondillo et al. 2015), at Skorpion there are chlorites strictly related to smectite. In Fig. 8A the chemical maps of Mg, Fe, Zn and Ca show Fe—Mg chlorite interleaved with smectite. Fig. 8B shows the occurrence of chlorite with a different composition, which could be ascribed to a possible baileychlore or to a contaminated Fe—Mg chlorite. In Fig. 9 are shown the electron diffraction patterns and the high-resolution images of the chlorite-bearing area of Fig. 8. In the patterns of Fig. 9A and B, chlorite presents a basal d-spacing of 14 Å. Fig. 9C and D illustrate the HRTEM images of the lattice fringe spacings of chlorite, thus confirming that d_{khl} of 14 Å is the most common spacing measured in the investigated areas. In some restricted areas, lower d-spacings can be observed, corresponding to

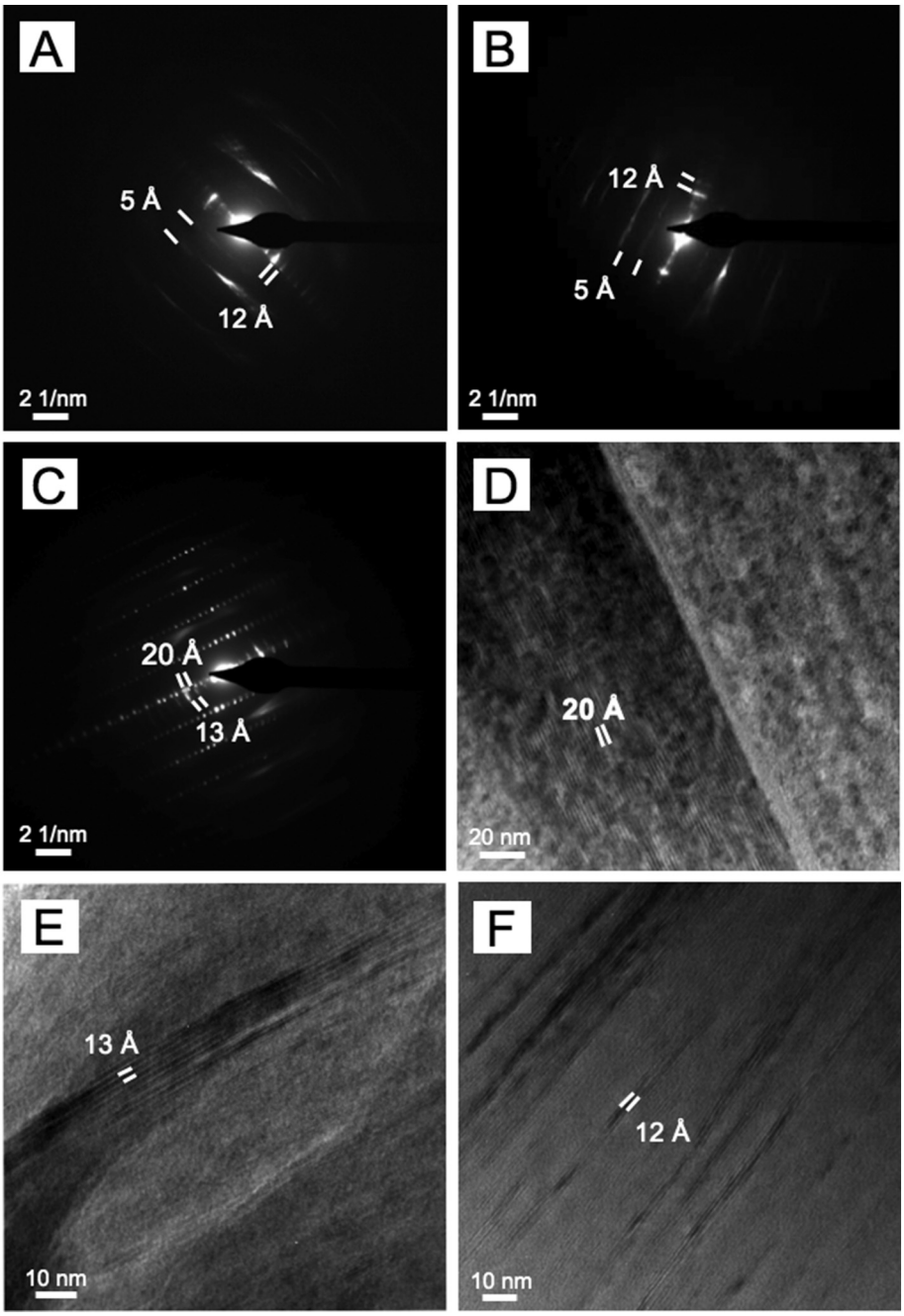

Fig. 5. (A), (B) Electron diffraction patterns of CCP of sample SK1, shown in Fig. 3A and B, respectively. (C) Electron diffraction patterns of mica (20 Å) associated with epitaxial smectite packet (12.5 Å) in sample SK3, and (D) HRTEM image of this mica. (E) HRTEM image of CCP sauconite in sample SK1, showing a close-up view of Fig. 3A. (F) HRTEM image of CCP epitaxial sauconite.

individual layers of smectite (Fig. 9C). Probably, the frequent open layers observed in HRTEM images, which are due to irradiation effects, correspond to smectitic layers, because this phenomenon is not usual in chlorite while largely affecting smectite. When a two-dimensional resolution is present, chlorite shows an ordered polytype (1 layer) at a local level, but a misorientation among the various packets occurs, which would produce an electron diffraction characteristic of disordered polytypes, as those visible in other images. This appears an ordered polytype at short range, but disordered at long range, a phenomenon not rare in phyllosilicates.

4.2. Chemical composition

It is well established that the AEM technique does not determine the absolute chemical composition of a mineral, but only the elemental ratios (i.e. Mondillo et al. 2015). Hence, the structural formulas of smectite and mica were calculated on the basis of 22 negative charges, i.e., $O_{10}(OH)_2$. According to the accepted stoichiometry of smectites (Güven 1988), Fe, that occurs in very small amounts (see below), was considered in bivalent form for trioctahedral species like sauconite (see also Buatier et al. 2016; Choulet et al. 2016; Kärner 2006). However, the occurrence of some Fe^{3+} cannot be excluded. The structural formulae of Skorpion sauconite are shown in Table 1. The silicon contents vary between 3.15 and 3.66 apfu. The content of the octahedral site is more variable, in an interval of 2.75 and 3.15 apfu; ^{VI}Al, Mg and Fe ranges are 0.00–0.59, 0.00–0.20 and 0.00–0.35 apfu, respectively. Most of the octahedral site is occupied by Zn, variable between 1.95 and 3.08 apfu. Among the interlayer cations, Ca is generally the only component, within a range of 0.05 and 0.19 apfu; K is detected in trace amounts or is absent. In Fig. 10A and B are shown the Zn-^{VI}Al-Fe + Mg and M^{+}-4Si-$3R^{2+}$ ternary plots, respectively; in the first plot it can be seen that the Skorpion sauconites are close to the Zn end-member, unlike the

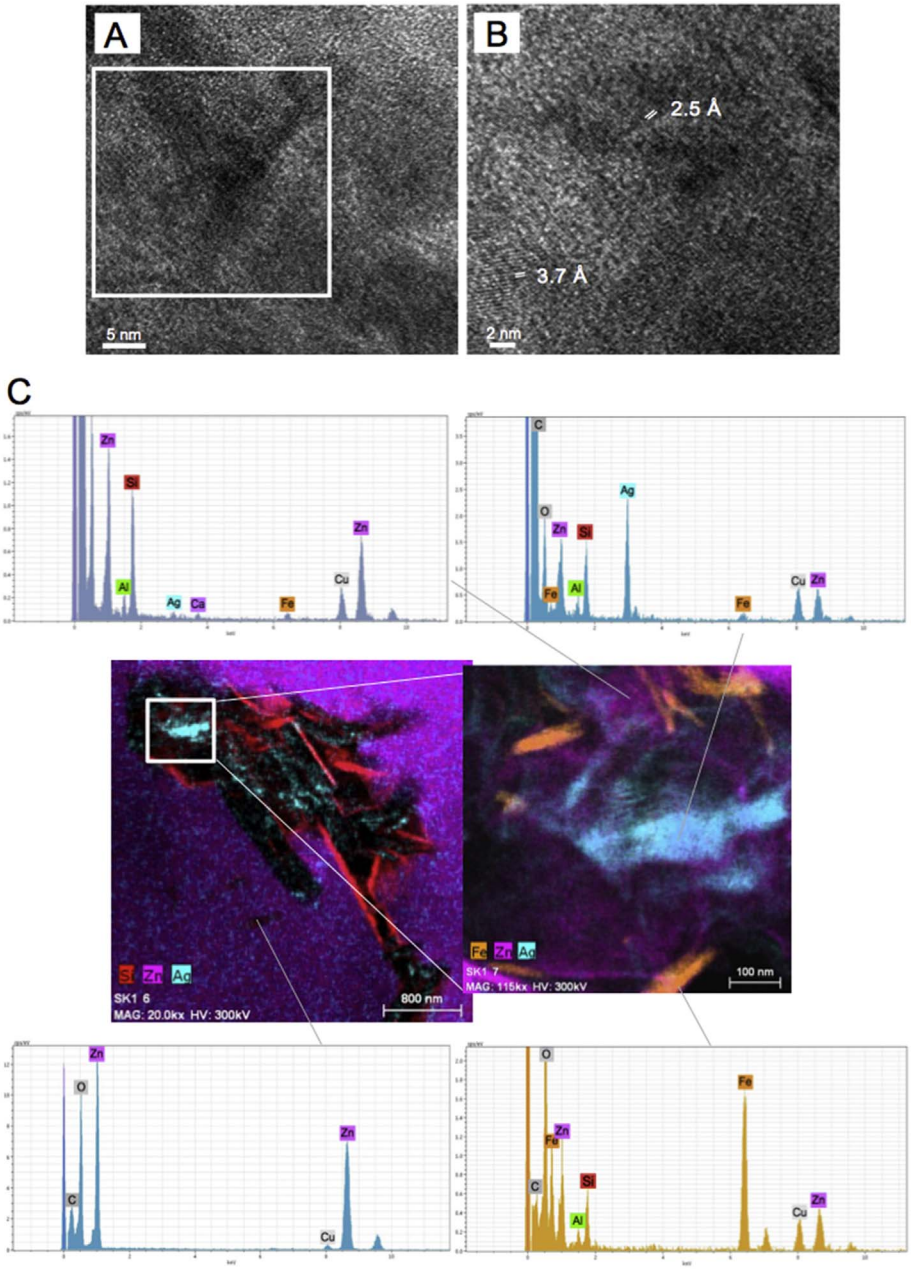

Fig. 6. (A) HRTEM of nanocrystalline hematite (sample SK1), and (B) enlargement of the area in the white frame. (C) Iron oxy-hydroxides coexisting with PCA smectite in sample SK1, together with Ag-rich areas (see text). Cu peak in the EDX spectra are due to copper ring attached to sample areas (see "Materials and Methods" paragraph).

Peruvian specimens that are chemically more variable. The sauconite considered in this study also partly overlap the compositional field of Kärner (2006). In the plot of Fig. 10B, used to distinguish the dioctahedral from the trioctahedral types (Meunier 2005), our data mainly plot around the theoretical sauconite composition (especially samples SK1 and SK8). The bivariate diagrams of selected elements are reported in Fig. 11A-C. In Fig. 11A the Al vs. Si correlation is shown, where the tetrahedral composition of the studied samples resulted nearly comparable with the Skorpion sauconites analysed by Kärner (2006) and more homogenous in respect to the Peruvian varieties of Mondillo et al. (2015). The same features can be observed in the plot Zn vs. ^{VI}Al (Fig. 11B), which clearly illustrates that the majority of the samples cluster in the area 3.0–2.5 apfu Zn and ^{VI}Al $<$ 0.5 apfu, and that the octahedral site is mainly filled by Zn (Table 1 and Fig. 10); moreover, a negative correlation between the two octahedral elements can be observed. The diagram Zn/Al vs. Si/Al illustrates a clear positive correlation, with a continuous variation of the two chemical parameters through the data. In this plot, the studied samples resulted more variable if compared with the data of Kärner (2006); this can by clearly explained by considering that the Kärner's data are averages on the bulk samples, while our data refer to many individual (nano)particles.

It is worth noting that sample SK8 can be considered almost a Ca-bearing end-member (Table 1), being K virtually lacking. This sample is also particularly homogenous (Figs. 10 and 11), as shown in the chemical map of Fig. 12. ICP-OES analysis was also carried out for sample SK8, in order to check on the Na content, not detectable either by TEM-AEM or by EDS-WDS when also Zn is present. The obtained chemical composition expressed in wt% is: SiO_2 37.93, Al_2O_3 6.23, FeO 0.01, MgO 0.40, CaO 1.55, Na_2O 0.20, K_2O 0.32, ZnO 38.75, LOI 15.11 (MnO, TiO_2 and P_2O_5 are below the detection limit). If reported in term of structural formula based on 22 negative charges (i.e. $O_{10}(OH)_2$), this composition is perfectly comparable to the compositions obtained by TEM-EDX for the same sample (Table 1).

Contrary to the Peruvian samples, at Skorpion we have detected very limited compositions likely attributable to Zn-beidellite, which was clearly recognized only in sample SK3 (Fig. 13). Table 2 reports one

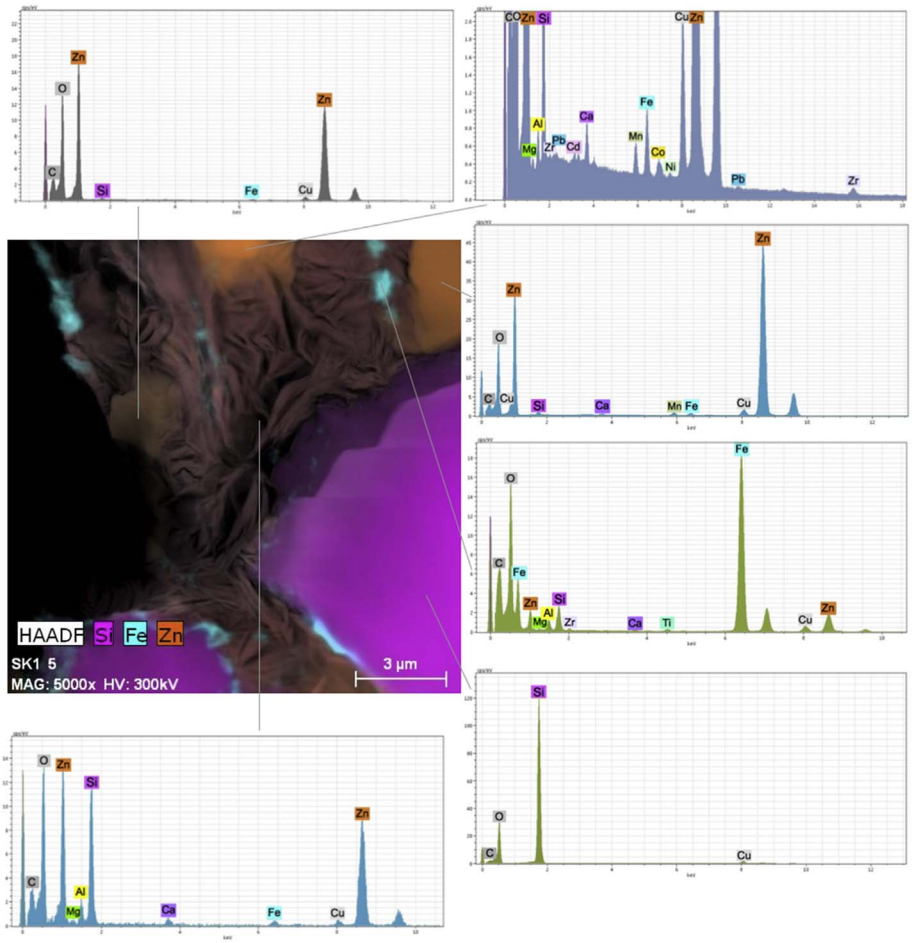

Fig. 7. Iron oxy-hydroxides coexisting with CCP smectite, together with a Zn-oxide (Cu peak as in Fig. 6).

beidellite-like composition; plotted in Figs. 10 and 11, this point-analysis falls in the beidellite field of Mondillo et al. (2015), whereas other analyses (indicated with dark triangles in the cited figures) show a mixed composition between sauconite and beidellite.

As illustrated in Figs. 8 and 9, chlorite was found in the Skorpion sample SK3. Table 2 shows two representative analyses of chlorites; the Fe−Mg chlorite could correspond to a chamosite, whereas as regards the baileychlore-like compositions, a contamination between sauconite and Fe−Mg chlorite cannot be excluded.

5. Discussion and conclusions

On the basis of the TEM-HRTEM study of Zn smectite-rich samples from the Skorpion deposit, some specific features can be evidenced for the “sauconite” and related minerals occurring in the nonsulfide orebody, when compared with the Peruvian clay associations reported in Mondillo et al. (2015):

(i) Skorpion sauconite is chemically more homogeneous if compared with natural sauconites from Accha and Yanque in Peru (Mondillo et al. 2015). In general, the composition of the Skorpion smectite is quite extreme, close to a Ca-rich end-member. Indeed the average composition of sauconite obtained by TEM-AEM corresponds to $Ca_{0.14}K_{0.02}(Zn_{2.7}Mg_{0.09}Al_{0.14}Fe_{0.10})(Si_{3.4}Al_{0.6})O_{10}(OH)_2{\cdot}nH_2O$. As regards the Na content, very small amounts were detected by ICP-OES in sauconite fraction of sample SK8, carefully selected for purity and with a compositionally homogeneous sauconite, as demonstrated by TEM-AEM investigation. Taking into account that ICP-OES is a bulk analysis, the result is very similar to chemical compositions obtained by TEM-AEM point-analyses. Hence, the Na content is not comparable to the much higher Ca amount, which is the major interlayer cation of the Skorpion smectites. The analyzed sauconites do not contain mobile elements like P, which, after the chemical data of Kärner (2006), would be released by the dissolution of apatite and subsequently precipitated as secondary phosphates (this has been rather the case) or retained in the clay structure. Other elements like Ti and REE, which could be similarly incorporated into the clays lattice, have not been detected in the analysed smectites but occur as single minerals, as testified by the occurrence of monazite and rutile observed in the studied samples.

(ii) Even though it is demonstrated that the Skorpion sauconite was also formed by replacement of hemimorphite, feldspar and smithsonite (Borg et al. 2003; Kärner 2006), in the studied samples the relationships between sauconite and micas resulted particularly significant. As a matter of fact, the structural support represented by detrital mica precursors is commonly observed in most samples, also in respect to the Peruvian case. Easy cleavage along the {001} planes of muscovite favored the epitaxial crystallization of Zn smectite on cleavage surfaces, as it has been observed also in other phyllosilicate associations (e.g. kaolinite-mica, Arostegui et al. 2001). This aspect can justify the extreme compositions of the studied samples: in fact, the fluids responsible for the clays deposition did not dissolve the mica crystals of detrital origin, which rather acted as a chemically inactive support. Consequently, the Zn clays are generally poor in Al and contain very low or no K and Mg. In the weathering profiles, alteration progressively affects the existing crystals, starting either from their boundaries and/or from cleavage planes. In the mica crystals, a volume increase which occurred perpendicularly to the mica lamellae, progressively caused their swelling and deformation that resulted in a sort of

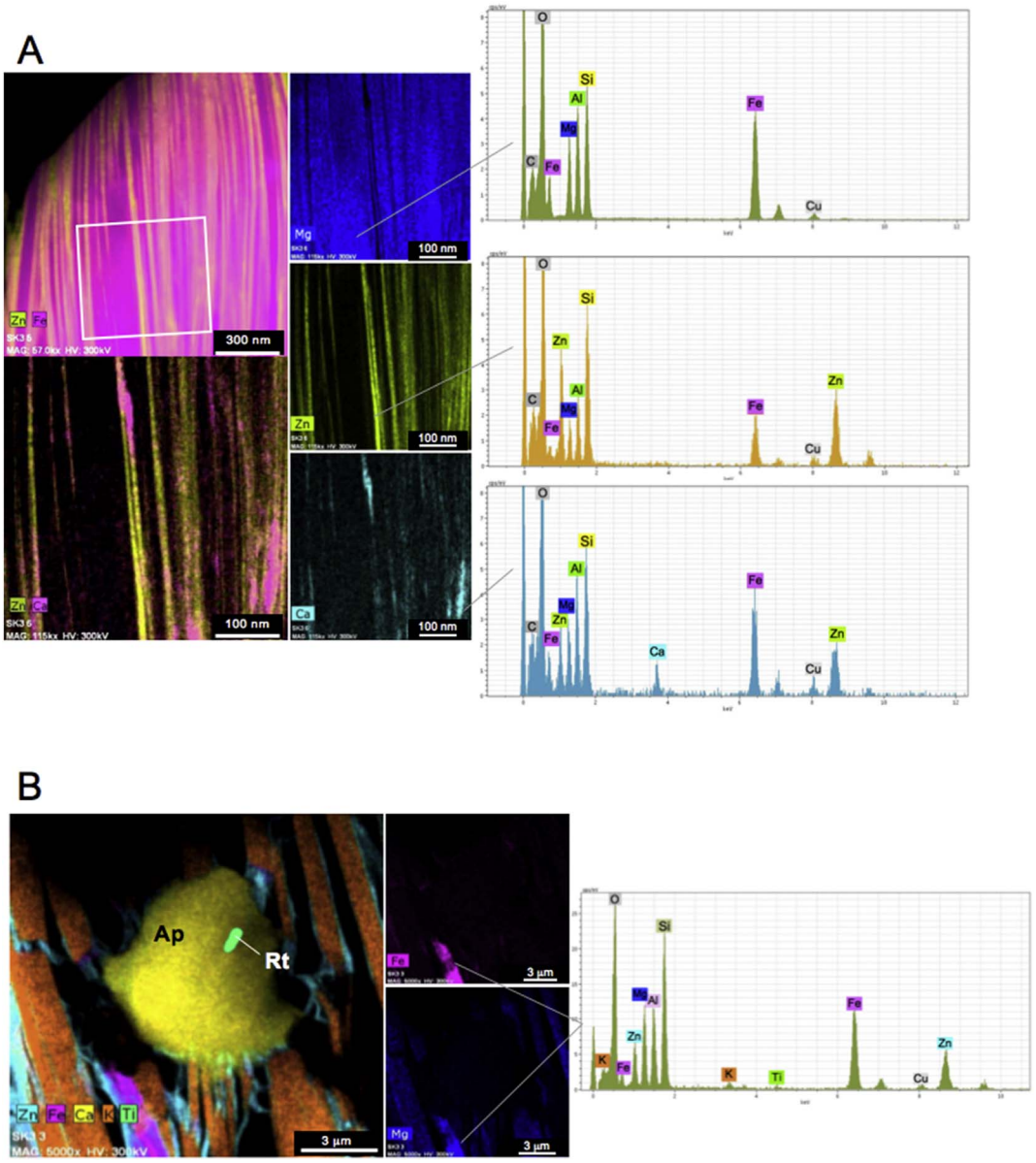

Fig. 8. (A) Mg-Fe-rich chlorite alternating with sauconite in sample SK3; the upper spectrum corresponds to a Mg-chlorite, the central and lower spectra could be interpreted as a combination of Zn-smectite and a likely Ca-bearing phyllosilicate of composition similar to vermiculite. (B) Mica with smectite in sample SK3; the area indicated by the spectrum could be a baileychlore-type phase (Cu peak as in Fig. 6). Mineral symbols as in Fig. 2.

"katamorphous" weathering type (Fitzpatrick 1984, and references therein). This process is enhanced by the fact that plastic smectites tend to flow and therefore to fill newly formed pores and cavities in the surrounding detrital and/or weathered minerals. However, a significant increase in volume can be also the result of the formation of hydrated minerals such as smectite, as well as hemimorphite and hydrozincite. As reported in the isocon diagram by Kärner (2006), a volume increase of 6% can be considered for the supergene Skorpion deposit.

(iii) In the studied samples, Zn-bearing beidellite was rarely observed in respect to the Peruvian occurrences, and some AEM analyses indicate, at least in part, mixed phases. A formula for Zn-beidellite corresponding to $K_{0.43}(Zn_{0.12}Mg_{028}Al_{1.40}Fe_{0.38})(Si_{3.44}Al_{0.56})O_{10}(OH)_2{\cdot}nH_2O$ could be nevertheless suggested. The chemical (i.e. K as the only interlayer cation) and textural characteristics of this dioctahedral clay seem to suggest that it formed directly at the expenses of micas, likely as an alteration product; then, beidellite might be formed through a process different from that responsible for the genesis of most sauconites. As shown in Fig. 13, a beidellitic smectite might firstly infiltrate the muscovite crystals; then sauconite crystallization follows, both on the mica cleavage surfaces and as void fillings.

(iv) Chlorite occurrence, not detected by bulk XRPD analyses, also distinguishes the studied samples. In general, the texture of the investigated chlorite-rich areas by AEM-HRTEM shows the same characteristics as the retrograde alteration of chlorite by smectite, firstly described by Nieto et al. (1994). The genetic relationship with chlorite is different than that with mica: mica is a simple template on which smectite crystallizes directly from fluids. The same fluids, however, were able to cause the chemical alteration of chlorite. This is not strange, as white mica is clearly more resistant than chlorite to chemical alteration. At Skorpion muscovite dominates over other micas within the original host rock; however, small amounts of biotite also occur, whose weathering could involve an alteration through mixed layer clay minerals or vermiculite, as proposed by Kärner (2006).

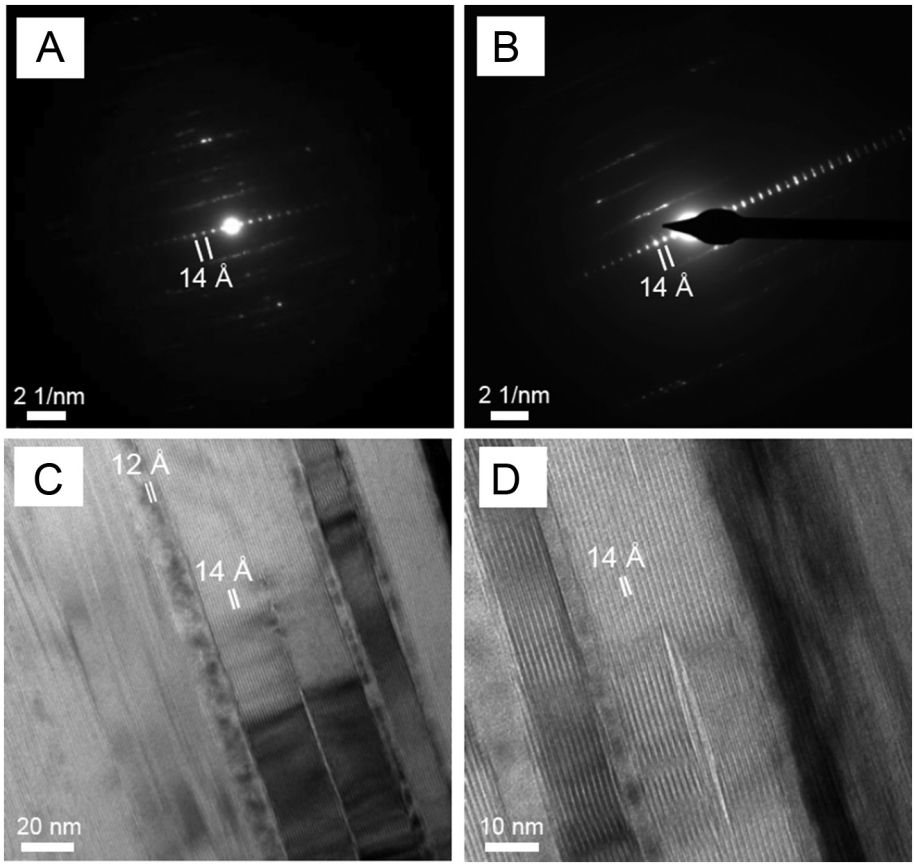

Fig. 9. (A) Electron diffraction of chlorite in sample SK3. (B) Example of a disordered chlorite polytype. (C) and (D) Lattice fringe images showing predominantly spacing of chlorite; some smectitic layers (12 Å) are shown in (C).

Table 1
Structural formulae of representative sauconite from Skorpion (Namibia), in atoms per formula unit (apfu), calculated on the basis on 12 anions $O_{10}(OH)_2$, obtained by AEM (analyses no. 1–20) and ICP-OES methods (analysis no. 21). See text for further explanations.

sample ID	SK1								SK3				SK8								
#	1	2	3	4	5	6	7	8	9	10	11	12	13	14	15	16	17	18	19	20	21 **ICP-OES**
Si	3.28	3.26	3.16	3.15	3.24	3.49	3.56	3.29	3.37	3.38	3.58	3.24	3.46	3.45	3.66	3.53	3.43	3.57	3.46	3.46	3.53
Al^{IV}	0.72	0.74	0.84	0.85	0.76	0.51	0.44	0.69	0.63	0.62	0.42	0.76	0.54	0.55	0.34	0.47	0.57	0.43	0.54	0.54	0.47
Al^{VI}	0.00	0.04	0.15	0.18	0.24	0.01	0.08	0.00	0.41	0.11	0.13	0.59	0.01	0.09	0.29	0.19	0.01	0.18	0.02	0.06	0.21
Mg	0.06	0.09	0.06	0.14	0.19	0.05	0.07	0.20	0.13	0.17	0.12	0.25	0.00	0.00	0.00	0.00	0.06	0.09	0.04	0.05	0.06
Fe^{2+}	0.16	0.21	0.19	0.19	0.15	0.11	0.11	0.11	0.35	0.12	0.06	0.14	0.00	0.00	0.00	0.00	0.01	0.01	0.01	0.01	0.02
Zn	2.88	2.70	2.76	2.58	2.42	2.85	2.72	2.84	1.95	2.70	2.74	1.77	3.08	2.98	2.57	2.76	3.06	2.72	3.03	2.94	2.66
$\Sigma_{octahedral}$	3.10	3.05	3.15	3.09	3.01	3.03	2.98	3.15	2.84	3.09	3.05	2.75	3.10	3.07	2.86	2.95	3.14	2.99	3.11	3.07	2.95
Ca	0.19	0.19	0.10	0.15	0.17	0.17	0.14	0.18	0.05	0.10	0.07	0.07	0.16	0.16	0.17	0.19	0.14	0.14	0.15	0.17	0.16
K	0.00	0.00	0.00	0.00	0.00	0.00	0.00	0.00	0.00	0.07	0.00	0.00	0.38	0.00	0.00	0.00	0.00	0.00	0.00	0.00	0.04
Na	–	–	–	–	–	–	–	–	–	–	–	–	–	–	–	–	–	–	–	–	0.04
$\Sigma_{interlayer}$	0.19	0.19	0.10	0.15	0.17	0.17	0.14	0.18	0.12	0.10	0.07	0.45	0.16	0.16	0.17	0.19	0.14	0.14	0.15	0.17	0.24
Σ_{charge}	0.38	0.39	0.20	0.30	0.34	0.33	0.28	0.37	0.18	0.21	0.15	0.52	0.33	0.31	0.33	0.38	0.29	0.27	0.29	0.34	0.40

_ Not determined.

(v) A possible Zn-oxide (not identified by XRPD) has been recorded in the Skorpion samples only by TEM-EDX; texturally, it seems to have been precipitated later than sauconite and at the same time of Fe-oxy-hydroxides. Even though observed only in sample SK1, this phase seems more capable of capturing various metals than the Fe-oxy-hydroxides. According to Paquet et al. (1986), the transition metals released by the destruction of the smectitic crystal lattices can be trapped by oxy-hydroxides and kaolinite during weathering in supergene environment. At Skorpion, Fe-oxy-hydroxides appear to be free of these metals; other trace metals (Co, Ni, Cr, Mn, Fe, Zr, Pb) seem to be concentrated in the Zn-oxide, or to form local enrichments (Ag), not related to oxy-hydroxides frameworks.

(vi) Fe-oxides (hematite) observed in this study crystallize after clay minerals (meteoric iron), forming very-low size domains.

As pointed out by Mondillo et al. (2015), the occurrence of (lesser) Zn-beidellite, chlorite, baileychlore, detrital micas and oxides at the micro- and nanoscale also in the Skorpion case study confirms the complex mineralogical nature of the Zn-nonsulfide smectite-rich (micro)systems. This feature can have remarkable implications for applied issues, like Zn production/mining processing in similar worldwide occurrences. At Skorpion, the leach/solvent extraction (SX)/electrowinning process route was adopted as processing method, allowing the production of zinc metal on site with Zn recoveries > 90%, without any

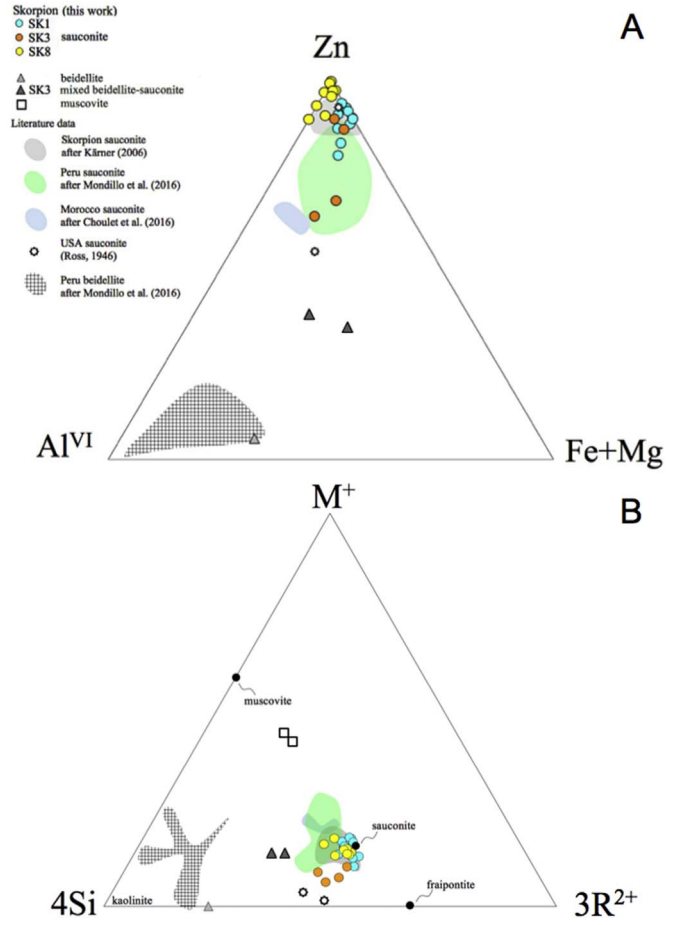

Fig. 10. (A) Zn-Al^{VI}-Fe + Mg diagram illustrating the octahedral chemical composition of sauconite and beidellite, as well as some examples of mixed compositions (dark grey triangles). (B) 4Si-M^{+}-$3R^{2+}$ diagram showing the trioctahedral and dioctahedral phases; the black dots represent the ideal mineral compositions. In both diagrams, our data are compared with literature data.

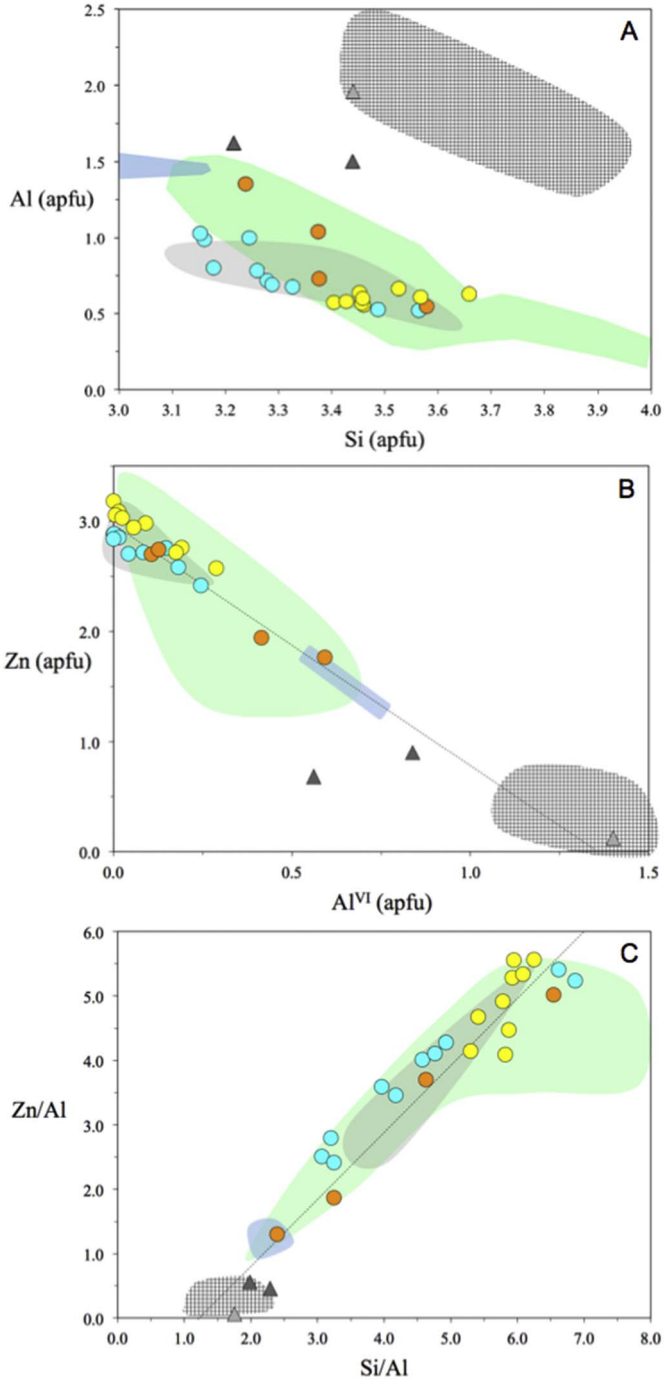

Fig. 11. Bivariate diagrams, illustrating some chemical features of the Skorpion samples (symbols as in Fig. 10).

apparent Zn loss due to the clay mineralogy (Cole and Sole 2002). Instead, the presence of different types of Zn-bearing clays can have a negative impact for Zn extraction from nonsulfide ores, when SX is not economically viable due to the presence of sulfuric acid consuming gangue minerals (de Wet and Singleton 2008). In fact, if gangue must be separated from the ore, for example through dense media separation or flotation, to achieve Zn concentration, the presence of several distinct Zn-bearing phyllosilicates makes more difficult to optimize the processing route (Boni et al., 2009a). If processing is not efficient, part of the ore is discarded together with gangue, and Zn recovery decreases, making the deposit not economically mineable.

The microtextures of the clays suggest two possible genetic mechanisms (Mondillo et al. 2015), i.e., smectites can grow on previous phyllosilicates (mica) (CCP texture), and/or directly nucleate and grow from solutions (PCA texture). Even though the geological environment of formation of these deposits is genetically related to supergene processes, a local control by a (likely low temperature) hydrothermal fluid on the precipitation of Zn-smectite should also be considered. Stable isotope measurements of Zn-rich clays in the Moroccan Bou Arhous Zn—Pb deposits (Choulet et al. 2016; Buatier et al. 2016) suggest that those Zn clay minerals formed by direct precipitation from fluids, which could be meteoric and/or hydrothermal. Also the TEM study of the Moroccan clays showed the occurrence of bent stacks of parallel platelets (tactoid) with different orientations suggesting direct precipitation from fluids.

At Skorpion, as in other worldwide occurrences, the supergene processes, consisting of surface oxidation at ambient temperatures of primary ore deposits remain the best-envisaged mechanism for the formation of nonsulfide Zn deposits. The Gariep belt area in Namibia, where the Skorpion deposit is located, experienced marked climate changes from Cretaceous onward, most likely from humid-tropical to semi-arid and arid conditions (Arfè et al. 2017). These climate changes controlled the formation and the nature of the supergene enrichment profile and would have created the most favorable conditions for the formation and variability of the clay minerals in this deposit (Boni and Mondillo 2015). Typical supergene processes at ambient temperatures with a tendency toward a dryer climate can be considered responsible for the genesis of the Skorpion sauconite, with the possible contribution of low T hydrothermal fluids.

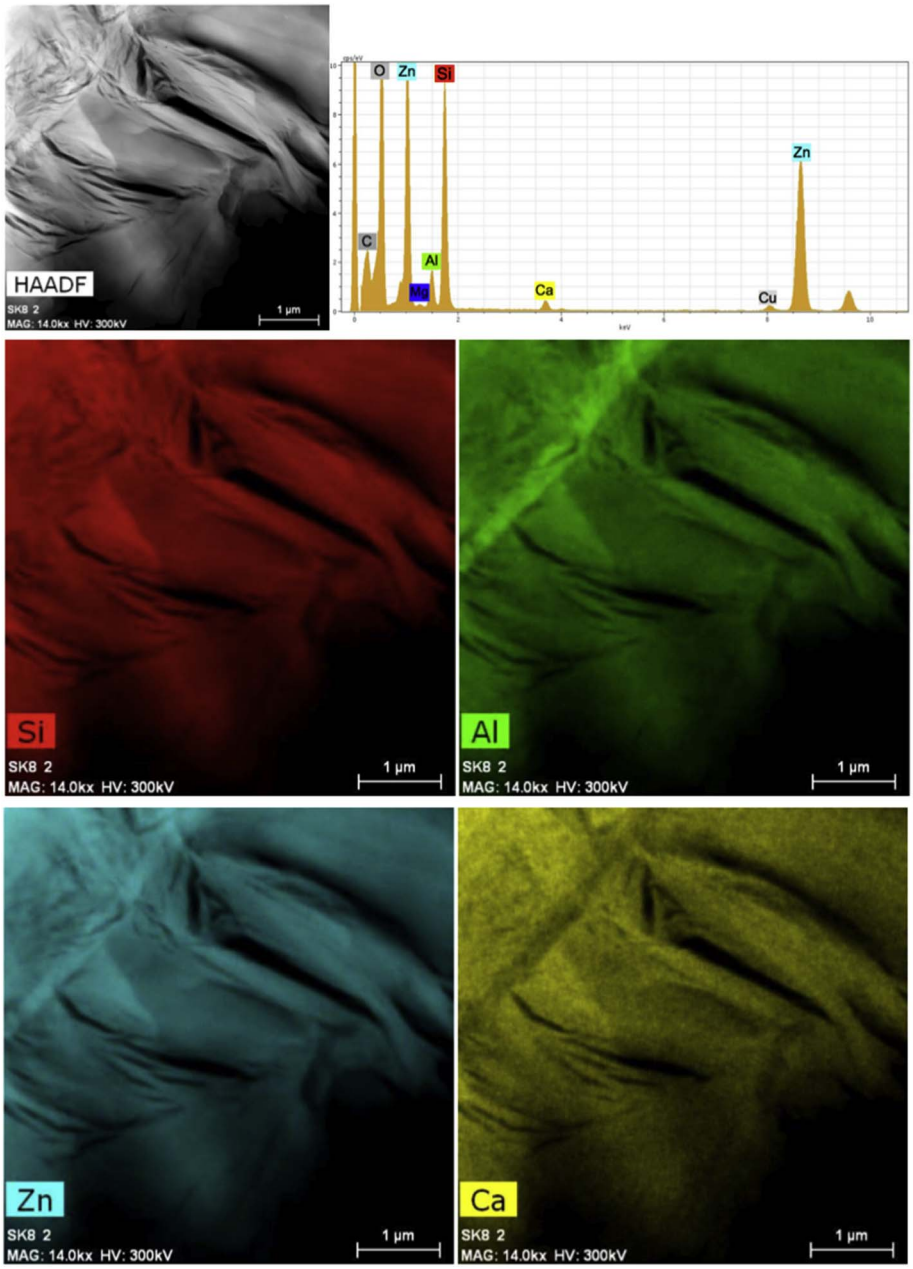

Fig. 12. HAADF image and chemical mapping of sample SK8.

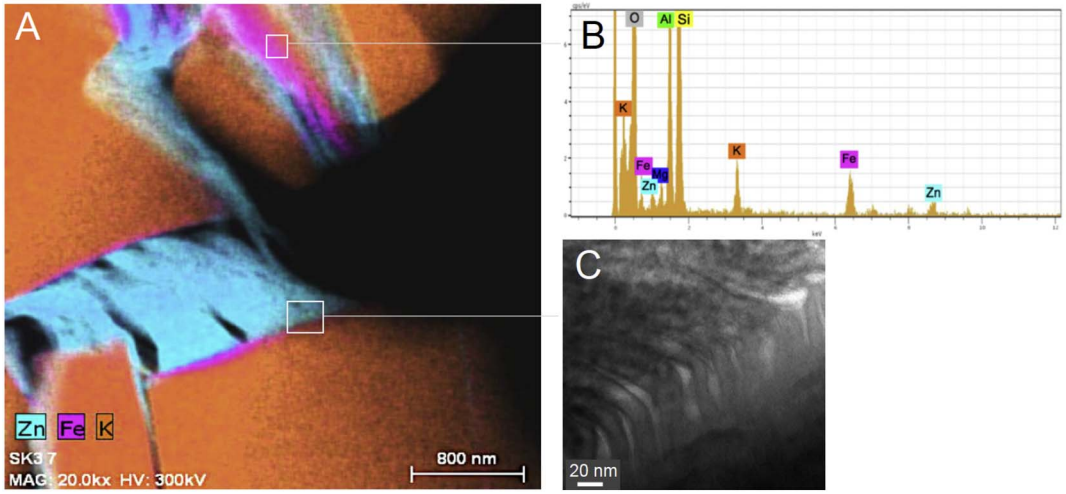

Fig. 13. (A) Chemical mapping and (B) qualitative EDX spectrum of a possible Zn-bearing beidellite in sample SK3. (C) Enlargement of a smectite-mica transition area.

Table 2
Structural formulae of representative beidellite, muscovite and chlorites from sample SK3, in atoms per formula unit (apfu), calculated on the basis on a total of 12 anions ($O_{10}(OH)_2$) for smectites and micas, and 18 anions ($O_{10}(OH)_8$) for chlorites.

sample ID	SK3						
	beidellite		muscovite			chlorite	
Si	3.440	Si	3.206	3.244	Si	3.144	2.783
Al^{IV}	0.560	Al	0.794	0.756	Al^{IV}	0.860	1.217
Al^{VI}	1.401	Ti	0.053	0.047	Al^{VI}	0.803	1.071
Mg	0.275	Al^{VI}	1.648	1.590	Mg	1.914	1.904
Fe^{3+}	0.378	Mg	0.309	0.389	Fe^{2+}	1.931	2.693
Zn	0.122	Fe^{3+}	0.017	0.020	Zn	0.967	0.000
$\Sigma_{octahedral}$	2.175	$\Sigma_{octahedral}$	2.027	2.046	Ca	0.063	0.000
					K	0.115	0.000
Ca	0.000	Ca	0.000	0.000	$\Sigma_{octahedral}$	5.794	5.669
K	0.430	K	0.968	1.007			
$\Sigma_{interlayer}$	0.430	$\Sigma_{interlayer}$	0.968	1.007			
Σ_{charge}	0.430						

Acknowledgements

The authors are indebted to the Skorpion personnel (Vedanta Ltd), and especially to the mine geologists for guidance at the mine sites and discussion. They are especially grateful to M.M. Abad (CIC, Granada) for the skilful support during TEM analyses and to R. de' Gennaro (DiSTAR, Napoli) for his help during SEM analyses. The authors thank E. Galán, Associated Editor of Applied Clay Science, and two anonymous referees for useful suggestions. This work was partly supported by Departmental funds (University of Napoli Federico II) of G. Balassone and M. Boni, and by the research projects CGL2011-30153 and CGL2016-75679-P from the Spanish Goverment and Research Group RNM-179 of the Junta de Andalucía,

References

Alchin, D.J., Moore, J.M., 2005. A review of the Pan-African, Neoproterozoic Rosh Pinah Zn-Pb deposit, southwestern Africa. South Africa. J. Geol. 108, 71–86.
Arfè, G., Boni, M., Balassone, G., Mondillo, N., Hinde,r G., Joachimski, M., 2017. New C-O isotopic data on supergene minerals from the Skorpion and Rosh Pinah ore deposits (Namibia): genetic and palaeoclimatic constraints. J. Afr. Earth Sci., 126,148–158.
Arostegui, J., Irabien, M.J., Nieto, F., Sangüesa, J., Zuluaga, M.C., 2001. Microtextures and the origin of muscovite-kaolinite intergrowths in sandstones of the Utrillas Formation, Basque Cantabrian Basin, Spain. Clays Clay Min. 49 (6), 529–539.
Balassone, G., Rossi, M., Boni, M., Stanley, G., McDermott, P., 2008. Mineralogical and geo- chemical characterization of nonsulfide Zn–Pb mineralization at Silvermines and Galmoy (Irish Midlands). Ore Geol. Rev. 33, 168–186.
Balassone, G., Nieto, F., Arfè, G., Boni, M., Mondillo, N., 2016. New investigations on Zn-clays from Skorpion (Namibia). 35th ICG Cape Town, SA.
Boland, M.B., Clifford, J.A., Meldrum, A.H., Poustie, A., 1992. Residual base metal and barite mineralization at Silvermines, Co. Tipperary, Ireland. In: Bowden, A.A., Earls, G., O'Connor, P.G., Pyne, J.F. (Eds.), The Irish Minerals Industry 1980–1990. Dublin, Ireland, pp. 247–260 Irish Association for Economic Geology.
Boni, M., Mondillo, N., 2015. The "Calamines" and the "Others": the great family of supergene nonsulfide zinc ores. Ore Geol. Rev. 67, 208–233.
Boni, M., Schmidt, P.R., DeWet, J.R., Singleton, J.D., Balassone, G., Mondillo, N., 2009a. Mineralogical signature of nonsulfide zinc ores at Accha (Peru): a key for recovery. Intern. J. Min. Proc. 93, 267–277.
Boni, M., Balassone, G., Arseneau, V., Schmidt, P., 2009b. The nonsulfide zinc deposit at Accha (Southern Peru): geological and mineralogical characterization. Econ. Geol. 104, 267–289.
Borg, G., Armstrong, R., 2002. Isotopic SHRIMP age dating of zircons from igneous basement and rhyolitic cover rocks at Skorpion, southern Namibia: IAGOD Symposium and Geocongress 2002, 11th quadriennial. Extended abstract vol, Windhoek, Geological Survey of Namibia.
Borg, G., Kärner, K., Buxton, M., Armstrong, R., van der Merwe, S.W., 2003. Geology of the Skorpion non-sulphide deposit, southern Namibia. Econ. Geol. 98, 749–771.
Buatier, M., Choulet, F., Petit, S., Chassagnon, R., Vennemann, T., 2016. Nature and origin of natural Zn clay minerals from the Bou Arhous Zn ore deposit: Evidence from electron microscopy (SEM-TEM) and stable isotope compositions (H and O. Appl. Clay Sci. 132, 377–390.
Choulet, F., Buatier, M., Barbanson, L., Guégan, R., Ennaciri, A., 2016. Zinc-rich clays in supergene non-sulfide zinc deposits. Mineral. Dep. 51, 467–490.
Cole, P.M., Sole, K.C., 2002. Solvent extraction in the primary and secondary recovery of zinc. In: Sole, K.C., Cole, P.M., Preston, J.S., Robinson, D.J. (Eds.), Proceedings International Solvent Extraction Conference ISEC 2002. South African Institute of Mining and Metallurgy, Johannesburg, pp. 863–870.
Coppola, V., Boni, M., Gilg, H.A., Balassone, G., Dejonghe, L., 2008. The "Calamine" nonsulfide Zn–Pb deposits of Belgium: petrographical, mineralogical and geochemical characterization. Ore Geol. Rev. 33, 187–210.
Davies, C.J., Coward, M.P., 1982. The structural evolution of the Gariep arc in southern Namibia (South-West Africa). Precambrian Res. 17, 137–197.
Emselle, N., McPhail, D.C., Welch, S.A., 2005. Reliance, Flinders Ranges: mineralogy, geochemistry and zinc dispersion around a nonsulfide orebody. Regolith 2005 – Ten Years of CRC LEME 86–90.
Fitzpatrick, E.A., 1984. Micromorpholgy of soils. Chapman and Hall, London New York (433 p).
Fransolet, A.M., Bourguignon, P., 1975. Données nouvelles sur la fraipontite de Moresnet (Belgique). Bull. Soc. Franç. Mineral. 98, 235–244.
Frimmel, H.E., 2000. The Pan-African Gariep belt in southwestern Namibia and western South Africa. Geological Survey of Namibia. Communications 12, 197–209.
Frimmel, H., Koller, F., Watkins, R.T., Faure, K., 1995. Tectonic history of mafic and ultramafic rocks in the Gariep Belt. Abstracts Centennial Geocongress, Geological Society South. Africa 226–229.
Frimmel, H.E., Fölling, P.G., Eriksson, P., 2002. Neoproterozoic tectonic and climatic evolution recorded in the Gariep Belt, Namibia and South Africa. Basin Res. 14, 55–67.
Frondel, C., 1972. The minerals of Franklin and Sterling Hill - A checklist. Wiley, New York (94 p).
Gallagher, K., Brown, R., 1999. The Mesozoic denudation history of the Atlantic margins of southern Africa and southeast Brazil and the relationship to offshore sedimentation. In: Cameron, N.R., Bate, R.H., Clure, V.S. (eds) The oil and gas habitats of the South Atlantic. Geol. Soc. Lond., Spec. Publ. 153, 41–53.
Garrels, R.M., Christ, C.L., 1990. Solutions, minerals, and equilibria. Lones and Bartlett Publishers, Boston (450 p).
Gresse, P.G., 1994. Strain partitioning in the southern Gariep arc as reflected by sheath folds and stretching directions. South. Afr. J. Geol. 97, 52–61.
Güven, N., 1988. Smectites: in Hydrous Phyllosilicates Exclusive of Micas, S. W. Bailey, ed., Reviews in Mineralogy 20, Mineralogical Society of America, Washington, D.C., 497-560.
Higashi, S., Miki, K., Komarneni, S., 2002. Hydrothermal synthesis of Zn smectite. Clay Clay Miner. 50, 299–305.
Hinder, G., 2015. Sensationeller Neufund von Churchit-(Y) aus der Skorpion Zink Mine in Namibia. Mineralien-Welt 26, 28–29.
Hye In Ahn, B.S., 2010. Mineralogy and Geochemistry of the Non-sulfide Zn Deposits in the Sierra Mojada District, Coahuila, Mexico. Unpublished Ph.D. Thesis, Austin. University of Texas, USA, pp. 193.
Jasper, M.J.U., Stanistreet, I.G., Charlesworth, E.G., 2000. Neoproterozoic inversion tectonics, half-graben depositories and glacial controversies, Gariep fold-thrust belt, southern Namibia. Geol. Surv. Namibia Comm. 12, 187–196.
Juillot, F., Morin, G., Ildefonse, P., 2003. Occurrence of Zn/Al hydrotalcite in smelter-impacted soils from northern France: evidence from EXAFS spectroscopy and chemical extractions. Am. Mineral. 88, 509–526.
Kärner, K., 2006. The metallogenesis of the Skorpion Non-sulphide Zinc Deposit, Namibia. Unpublished Ph.D. Thesis, Martin-Luther-Universität Halle-Wittenberg (Germany), pp. 133.
Kaufhold, S., Färber, G., Dohrmann, R., Ufer, K., Grathoff, G., 2015. Zn-rich smectite from the Silver Coin Mine, Nevada, USA. Clay Min. 50, 417–430.
King, L.C., 1951. South African Scenery. Oliver and Boyd, London (379 p).
Kloprogge, T., Komarneni, S., Amonette, J., 1999. Synthesis of smectite clay minerals: a critical review. Clay Clay Miner. 47, 529–554.
Manceau, A., Lanson, B., Schlegel, M.L., Harge, J.C., Musso, M., Eybert-Berard, L., Hazemann, J.L., Chateigner, D., Lamble, G.M., 2000. Quantitative Zn speciation in smelter-contaminated soils by EXAFS spectroscopy. Amer. J. Sci. 300, 289–343.
Mondillo, N., Boni, M., Balassone, G., Villa, I.M., 2014. The Yanque Prospect (Peru): from polymetallic Zn-Pb mineralization to a nonsulfide deposit. Econ. Geol. 109, 1735–1762.
Mondillo, N., Nieto, F., Balassone, G., 2015. Micro- and nano-characterization of Zn-clays in nonsulfide supergene ores of southern Peru. Am. Mineral. 100, 2484–2496.
Newman, A.C.D., Brown, G., 1987. The chemical constitution of clays. In: Newman,

A.C.D. (Ed.), Chemistry of Clays and Clay Minerals. John Wiley & Sons, New York (128 p).
Nieto, F., Velilla, N., Peacor, D.R., Huertas, M.O., 1994. Regional retrograde alteration of sub-greenschist facies chlorite to smectite. Contr. Mineral. Petrol. 115, 243–252.
Page, D.C., Watson, M.D., 1976. The Pb-Zn deposit of Rosh Pinah Mine, South West Africa. Econ. Geol. 71, 306–327.
Paquet, H., Colin, F., Duplay, J., Nahon, D., Millot, G., 1986. Ni, Mn, Zn, Cr-smectites, early and effective traps for transition elements in supergene ore deposits. – In: Rodriguez-Clemente & Tardy, Y. (eds.): Proceedings of the International Meeting "Geochemistry of the earth surface and processes of mineral formation", Granada (Spain), 16 – 22 March 1986. In: 221–229.
Partridge, T.C., 1998. Of diamonds, dinosaurs and diastrophism: 150 million years of landscape evolution in southern Africa. South. Afr. J. Geol. 101, 167–184.
Partridge, T.C., Maud, R.R., 1987. Geomorphic evolution of southern Africa since the Mesozoic. S. Afr. J. Geol. 90, 179–208.
Pascua, C.S., Ohnuma, M., Matsushita, Y., Tamura, K., Yamada, H., Cuadros, J., Ye, J., 2010. Synthesis of monodisperse Zn-smectite. Appl. Clay Sci. 48, 55–59.
Petit, S., Righi, D., Decarreau, A., 2008. Transformation of synthetic Zn stevensite to Zn-talc induced by the Hofmann-Klemen effect. Clay Clay Miner. 56, 645–654.
Reid, D.L., Ransome, I.G.D., Onstott, T.C., Adams, C.J., 1991. Time of emplacement and metamorphism of late Precambrian mafic dikes associated with the Pan-African Gariep orogeny, southern Africa: implications for the age of the Nama Group. J. Afr. Earth Sci. 13, 531–541.
Ross, C.S., 1946. Sauconite - a clay mineral of the Montmorillonite group. Am. Mineral. 31, 411–424.
Rule, A.C., Radke, F., 1988. Baileychlore, the Zn end member of the trioctahedral chlorite series. Am. Mineral. 73, 135–139.
Scott, K.M., 1986. Elemental partitioning into Mn- and Fe-oxides derived from dolomitic shale-hosted Pb-Zn deposits, Northwest Queensland, Australia. Chem. Geol. 57, 395–414.
Sherman, D.M., 2001. Weathering Reactions and Soil-Groundwater Chemistry. Environmental Geochemistry, University of Bristol, Unpubl. Lecture Notes 2001 (/2002), 11.
Stanistreet, I.G., Kukla, P.A., Henry, G., 1991. Sedimentary basinal response to a late Precambrian Wilson cycle: The Damara orogen and Nama foreland, Namibia. J. Afr. Earth Sci. 13, 141–156.
van Vuuren, C.J.J., 1986. Regional setting and structure of the Rosh Pinah zinc-lead deposit, South West Africa/Namibia. In: Anhaeusser, C.R., Maske, S. (Eds.), Mineral deposits of southern Africa, vol. II, Geological Society of South Africa, Johannesburg, pp. 1593–1607.
de Wet, K., Singleton, J.D., 2008. Development of a viable process for the recovery of zinc from oxide ores. The Southern African Institute of Mining and Metallurgy, Proceedings of LEAD and ZINC '08, Durban, 177–192.
Whitney, D.L., Evans, B.W., 2010. Abbreviations for names of rock-forming minerals. Am. Mineral. 95, 185–187.